
# Dimensional splitting with unconditional stability for advection on a sphere

W.H. Hundsdorfer, E.J. Spee

Department of Numerical Mathematics

**Report NM-R9416 July 1994**

CWI is the National Research Institute for Mathematics and Computer Science. CWI is part of the Stichting Mathematisch Centrum (SMC), the Dutch foundation for promotion of mathematics and computer science and their applications.
SMC is sponsored by the Netherlands Organization for Scientific Research (NWO). CWI is a member of ERCIM, the European Research Consortium for Informatics and Mathematics.


P.O. Box 94079, 1090 GB Amsterdam (NL)
Kruislaan 413, 1098 SJ Amsterdam (NL)
Telephone +31 20 592 9333
Telefax +31 20 592 4199

# Dimensional Splitting with Unconditional Stability for Advection on a Sphere

W. Hundsdorfer and E.J. Spee
*CWI*
*P.O. Box 94079, 1090 GB Amsterdam, The Netherlands*

**Abstract**

In this paper we consider some dimensional splitting schemes for horizontal advection on a sphere with a uniform longitude-latitude grid. The 1D subprocesses that arise within the splitting are solved with an explicit finite-volume type scheme, which is made unconditionally stable by allowing the stencil to vary with the Courant numbers. For the inaccuracies at the poles some special measures are discussed. The results are compared with tests of Smolarkiewicz & Rasch [8].

*1991 Mathematics Subject Classification*: 65M06, 65M12, 65M25.
*1991 CR Categories*: G1.8.
*Keywords & Phrases*: hyperbolic PDEs, linear advection, dimensional splitting, flux limiting.

*Note*: Background research for the project CIRK. Financial support from RIVM and CRAY Research Inc. (under grant CRG 94.01 via the Stichting Nationale Computerfaciliteiten, NCF) is acknowledged.

## 1. Introduction

The subject of this paper is the numerical solution of horizontal advection on a sphere for a concentration, or vector of concentrations, $c(t, \lambda, \phi)$ on a uniform longitude-latitude grid. The mathematical equation describing the advection is given by

$$\frac{\partial c}{\partial t} + \frac{1}{a\cos(\phi)}\left(\frac{\partial (uc)}{\partial \lambda} + \frac{\partial (\cos(\phi) vc)}{\partial \phi}\right) = 0, \tag{1.1}$$

where $\lambda \in [0, 2\pi)$ and $\phi \in [-\pi/2, \pi/2]$ are the longitude and latitude coordinates, $a$ is the radius of the sphere, and $u, v$ the given wind velocities (in meter per second) in the latitudinal and longitudinal direction, respectively. The efficient solution of such equations is one of the main numerical difficulties for modeling global transport of trace constituents in the troposphere.

The advection equation (1.1) becomes singular at the poles $\phi = \pm\pi/2$, due to the underlying mapping of the sphere on the $\lambda, \phi$-plane. This may cause inaccuracies in numerical schemes as well as stability problems. A thorough review with many references can be found in Williamson [11]. Along with the usual requirements, such as accuracy and computational efficiency, it is also important in many applications to have positivity, since negative values may lead to instability when advection is combined with nonlinear chemistry.

Report NM-R9416
ISSN 0169-0388
CWI
P.O. Box 94079, 1090 GB Amsterdam, The Netherlands

In this paper we consider a scheme based on dimensional splitting. The 1D subprocesses that arise within the splitting are solved with an explicit third-order finite-volume type scheme, used in [3] for planar advection. Positivity is obtained by flux-limiting. The scheme is made unconditionally stable by allowing the stencil to vary with the local Courant numbers. In this way, small time steps near the poles can be avoided.

However, due to the large Courant numbers, accuracy near the poles remains a problem with this approach. To suppress these inaccuracies we shall propose two modifications, namely mixing inside polar caps and deformation corrections (where the scheme is corrected such that background concentrations are not deformed). With both modifications the results are satisfactory. The resulting schemes have good shape preserving properties, they are positive and appear to be very efficient in terms of computational costs versus accuracy. Comparisons will be made with the semi-Lagrangian methods of Smolarkiewicz and Rasch [8] for a solid body rotation test on the sphere.

In Section 2 some results of [3], concerning advection on a plane, are reviewed and the extension to unconditional stability is discussed. Section 3 contains the tests for advection on the sphere, with modifications at the poles and numerical comparisons.

## 2. Planar advection

### *2.1. Unconditional stability for 1D advection*

For the 1D advection equation

$$c_t + (uc)_x = 0, \tag{2.1}$$

with subscripts $t, x$ denoting partial derivatives, we consider numerical schemes in conservation form

$$c_i^{n+1} = c_i^n + \left( F^n_{i-\frac{1}{2}} - F^n_{i+\frac{1}{2}} \right). \tag{2.2}$$

Here $c_i^n$ approximates the average value of $c(t,x)$ over the cell $\Omega_i = (x_{i-\frac{1}{2}}, x_{i+\frac{1}{2}})$ at time $t_n = n\Delta t$, and $F^n_{i-\frac{1}{2}}, F^n_{i+\frac{1}{2}}$ give the inflow and outflow at the cell boundaries. The grid will be assumed to be equidistant, with cell centers $x_i = i\Delta x$, but generalizations to arbitrary grids are easily obtained. In the following the superscripts $n$ are omitted.

For the computation of the fluxes $F_{i+\frac{1}{2}}$ we shall allow the stencil to vary with the Courant number. In this way it is easy to achieve unconditional stability while maintaining explicitness of the scheme. For example, the first-order upwind, donor cell scheme, is given by

$$F_{i+\frac{1}{2}} = \begin{cases} \nu_{i+\frac{1}{2}} c_i & \text{if} \quad u_{i+\frac{1}{2}} \geq 0, \\ -\nu_{i+\frac{1}{2}} c_{i+1} & \text{if} \quad u_{i+\frac{1}{2}} < 0 \end{cases}$$

with $\nu_{i+\frac{1}{2}} = |u_{i+\frac{1}{2}}|\Delta t/\Delta x$ the local Courant number at the cell boundary $x_{i+\frac{1}{2}}$. In this form the scheme is stable under the CFL restriction $\max_i \nu_{i+\frac{1}{2}} \leq 1$. The stability restriction is avoided by taking

$$F_{i+\frac{1}{2}} = \begin{cases} \tilde{\nu}_{i+\frac{1}{2}} c_{i-k} + (c_{i-k+1} + \cdots + c_i) & \text{if} \quad u_{i+\frac{1}{2}} \geq 0, \\ -\tilde{\nu}_{i+\frac{1}{2}} c_{i+k+1} - (c_{i+1} + \ldots + c_{i+k}) & \text{if} \quad u_{i+\frac{1}{2}} < 0, \end{cases}$$

where

$$k = k_{i+\frac{1}{2}} = \lfloor \nu_{i+\frac{1}{2}} \rfloor \quad \text{and} \quad \tilde{\nu}_{i+\frac{1}{2}} = \nu_{i+\frac{1}{2}} - k_{i+\frac{1}{2}}, \tag{2.3}$$

and $\lfloor \nu \rfloor$ denotes the largest integer $\leq \nu$. Inserting this into (2.2), we see that for constant $u$ the same formula as for Courant numbers $\leq 1$ is applied, together with a shift over $k$ gridpoints. Therefore the scheme will be unconditionally stable (for constant $u$). This is similar as with semi-Lagrangian methods, but due to the conservation form of the scheme we maintain mass conservation.

Instead of first-order upwind we shall use a third-order upwind-biased scheme. Let

$$d_0(\nu) = \frac{1}{6}(2-\nu)(1-\nu), \quad d_1(\nu) = \frac{1}{6}(1-\nu^2). \tag{2.4}$$

If $u_{i+\frac{1}{2}} \geq 0$ we set

$$F_{i+\frac{1}{2}} = \tilde{\nu}_{i+\frac{1}{2}}\Big(c_{i-k} + d_0(\tilde{\nu}_{i+\frac{1}{2}})(c_{i+1-k} - c_{i-k}) + d_1(\tilde{\nu}_{i+\frac{1}{2}})(c_{i-k} - c_{i-1-k})\Big) + \sum_{l=i-k+1}^{i} c_l \tag{2.5}$$

whereas for $u_{i+\frac{1}{2}} < 0$,

$$F_{i+\frac{1}{2}} = -\tilde{\nu}_{i+\frac{1}{2}}\Big(c_{i+k+1} + d_0(\tilde{\nu}_{i+\frac{1}{2}})(c_{i+k} - c_{i+k+1}) + d_1(\tilde{\nu}_{i+\frac{1}{2}})(c_{i+k+1} - c_{i+k+2})\Big) - \sum_{l=i+1}^{i+k} c_l \tag{2.6}$$

with $k = k_{i+\frac{1}{2}}$ and $\tilde{\nu}_{i+\frac{1}{2}}$ given by (2.3).

If $u$ is constant and the Courant number is bounded by 1 the scheme reduces to the third-order scheme which uses a 4-point upwind biased stencil. It was shown by Strang [9] that schemes of this optimal-order type are stable up to Courant number equal to 1. Unconditional stability, for constant $u$, of the above formula follows again by observing that we apply in fact the same formula as for Courant number $\leq 1$, only on a shifted stencil.

To ensure positivity we will use a Sweby-type flux limiter (see [10, 13, 6, 4] for example). Detailed motivation for the particular limiter used here can be found in [3]. The limiter is based on the ratios

$$\theta_i = \frac{c_i - c_{i-1}}{c_{i+1} - c_i}$$

and the limiter function is

$$\psi(\nu,\theta) = \max\Big(\ 0\ ,\ \min\Big(\ 1\ ,\ d_0(\nu) + d_1(\nu)\theta\ ,\ \frac{1-\nu}{\nu}\theta\ \Big)\Big). \tag{2.7}$$

In actual computations a small number, for example $10^{-10}$, is added to the denominators of $\theta$ and $(1-\nu)/\nu$ to avoid division by zero. The limited scheme reads as follows: if $u_{i+\frac{1}{2}} > 0$ then $F_{i+\frac{1}{2}}$ is computed from

$$F_{i+\frac{1}{2}} = \tilde{\nu}_{i+\frac{1}{2}}\Big(c_{i-k} + \psi(\tilde{\nu}_{i+\frac{1}{2}}, \theta_{i-k})(c_{i+1-k} - c_{i-k})\Big) + \sum_{l=i-k+1}^{i} c_l, \tag{2.8}$$

with $k = k_{i+\frac{1}{2}}$ and $\tilde{\nu}_{i+\frac{1}{2}}$ as before, and if $u_{i+\frac{1}{2}} < 0$ we use

$$F_{i+\frac{1}{2}} = -\tilde{\nu}_{i+\frac{1}{2}}\Big(c_{i+k+1} + \psi(\tilde{\nu}_{i+\frac{1}{2}}, \frac{1}{\theta_{i+k+1}})(c_{i+k} - c_{i+k+1})\Big) - \sum_{l=i+1}^{i+k} c_l. \tag{2.9}$$

Note that with $\psi(\nu,\theta) = d_0(\nu) + d_1(\nu)\theta$ the original, unlimited scheme would have been reobtained.

The above formulas depend, through $\nu_{i+\frac{1}{2}}$, on the velocity $u_{i+\frac{1}{2}}$. From a physical interpretation of the flux form (2.2), in terms of inflow and outflow for the cells, it follows that $u_{i+\frac{1}{2}}$ should be taken as $(x_{i+\frac{1}{2}} - \bar{x}_{i+\frac{1}{2}})/\Delta t$, where $\bar{x}_{i+\frac{1}{2}}$ is the departure point at time $t_n$ of the characteristic $x'(t) = u(t, x(t))$ which passes through $x_{i+\frac{1}{2}}$ at time $t_{n+1}$ (see [3], for instance). Therefore, if we take simply $u_{i+\frac{1}{2}} = u(x_{i+\frac{1}{2}})$ the order will only be 1 for non-constant velocities. In this paper we will apply the second-order formula

$$u_{i+\frac{1}{2}} = \left(u - \frac{1}{2}\Delta t\, u_x u\right)(x_{i+\frac{1}{2}}). \tag{2.10}$$

The derivatives $u_x$ appearing here are computed by second-order difference quotients.

Higher order approximations for the departure point could be easily derived, as well as modifications in case $u$ also varies in time, see [3]. However, we shall apply the 1D scheme within a second-order splitting setting and in our applications the windfields will be held constant for fairly long time intervals.

*2.2. Second-order splittings*

To solve the 2D advection equation on a plane

$$c_t + (uc)_x + (vc)_y = 0, \tag{2.11}$$

we consider dimensional splitting. In it simplest form this reads as follows: if $c_n(x,y)$ is an approximation to the exact solution at time $t_n$, we solve subsequently

$$\begin{aligned} c^*_t + (uc^*)_x = 0 \quad (t_n \le t \le t_{n+1}), \qquad & c^*(t_n,x,y) = c_n(x,y), \\ c^{**}_t + (vc^{**})_y = 0 \quad (t_n \le t \le t_{n+1}), \qquad & c^{**}(t_n,x,y) = c^*(t_{n+1},x,y), \end{aligned} \tag{2.12}$$

giving a new approximation $c_{n+1}(x,y) = c^{**}(t_{n+1},x,y)$ at time level $t_{n+1}$.

It is well known that this type of splitting will introduce a first-order temporal error. In fact, by a simple analysis [3] it follows that the splitting procedure will solve the *modified* equation

$$c_t + (\underline{u}c)_x + (\underline{v}c)_y = \mathcal{O}(\Delta t^2)$$

with perturbed velocities

$$\underline{u} = u - \frac{1}{2}\Delta t\, u_y v, \qquad \underline{v} = v + \frac{1}{2}\Delta t\, u v_x.$$

It follows that second-order splitting is achieved by using in the splitting procedure not the original velocities $u$ and $v$, but instead

$$\overline{u} = u + \frac{1}{2}\Delta t\, u_y v, \qquad \overline{v} = v - \frac{1}{2}\Delta t\, u v_x. \tag{2.13}$$

This precisely counteracts the first-order perturbations in the above modified equation.

As observed by Bott [2], first-order splitting may give qualitatively bad results with deformational flow fields. We have repeated the experiment of [2] (on the deformation test of [7] with background): in the flow field described by the stream function

$$\varphi(x,y) = 8\sin\left(\frac{\pi x}{25}\right)\cos\left(\frac{\pi y}{25}\right), \quad 0 \le x,y \le 100,$$

with $u = -\varphi_y$ and $v = \varphi_x$, a cone with center $(x,y) = (50,50)$, base radius 15 and height 4 is placed on top of a background concentration equal to 1. In this flow, the cone should be strongly deformed but the background should remain constant since the velocity field is divergence-free.

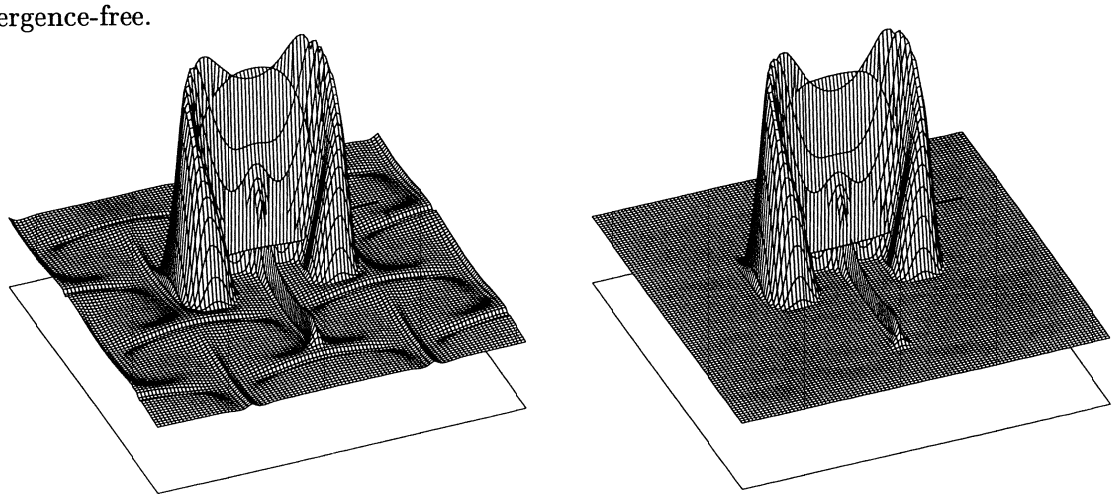

FIGURE 1. First-order (left) and second-order splitting (right) in deformation test

In Figure 1 the numerical solutions are displayed for first-order and second-order splitting, with $\Delta t = 0.7$ and $\Delta x = \Delta y = 1$ after 38 time steps. The fractional steps are solved by the limited scheme discussed in the previous section. With first-order splitting we use the velocities at cell interfaces according to (2.10), that is

$$u_{i\pm\frac{1}{2},j} = \left(u - \frac{1}{2}\Delta t\, u_x u\right)(x_{i\pm\frac{1}{2}}, y_j), \quad v_{i,j\pm\frac{1}{2}} = \left(v - \frac{1}{2}\Delta t\, v_y v\right)(x_i, y_{j\pm\frac{1}{2}}).$$

For the second-order splitting we also take into account the modification (2.13), which leads to

$$\begin{aligned} u_{i\pm\frac{1}{2},j} &= \left(u - \tfrac{1}{2}\Delta t\, u_x u + \tfrac{1}{2}\Delta t\, u_y v\right)(x_{i\pm\frac{1}{2}}, y_j), \\ v_{i,j\pm\frac{1}{2}} &= \left(v - \tfrac{1}{2}\Delta t\, v_y v - \tfrac{1}{2}\Delta t\, u v_x\right)(x_i, y_{j\pm\frac{1}{2}}). \end{aligned} \tag{2.14}$$

It is clear from Figure 1 that with first-order splitting not only the cone but also the background concentration is strongly deformed (without the modification (2.10) it is even worse, similar to Figure 9b in [2]). This deformation is caused by the fact that the modified equation is no longer divergence-free. The result with second-order splitting is satisfactory. Although there still is a slight deformation of the background concentration, this is hardly visible anymore.

**Remark.** Second-order accuracy is also achieved with the so-called Strang splitting [6],

$$\begin{aligned} c_t^* + (uc^*)_x = 0 \quad (t_n \le t \le t_{n+\frac{1}{2}}), \qquad & c^*(t_n, x, y) = c_n(x, y), \\ c_t^{**} + (vc^{**})_y = 0 \quad (t_n \le t \le t_{n+1}), \qquad & c^{**}(t_n, x, y) = c^*(t_{n+\frac{1}{2}}, x, y), \\ c_t^{***} + (uc^{***})_x = 0 \quad (t_{n+\frac{1}{2}} \le t \le t_{n+1}), \qquad & c^{***}(t_{n+\frac{1}{2}}, x, y) = c^{**}(t_{n+1}, x, y), \end{aligned}$$

where now $c^{***}(t_{n+1}, x, y)$ gives the new approximation at time level $t_{n+1}$. In some tests we found little difference between this form of splitting and the form (2.12) with modified wind field (2.14). If at each time level $t_n$ output is demanded, then Strang splitting will be more expensive. In the following, we therefore consider splitting with the modified wind field (2.14).

## 3. Advection on the sphere

### *3.1. The splitting scheme*

Consider the advection equation (1.1) on a sphere. In the following we denote, for brevity, $\Gamma = \cos(\phi)$. The dimension of the velocities $u, v$ is meter per second. The relevant velocities on the $\lambda, \phi$-plane are

$$U = \frac{u}{a\Gamma} \quad \text{and} \quad V = \frac{v}{a}. \tag{3.1}$$

Note that $U$ becomes very large near the poles, reflecting the fact that the mesh width on the sphere in the $\lambda$-direction becomes small.

Equation (1.1) can be written as

$$\frac{\partial c}{\partial t} + \frac{\partial (Uc)}{\partial \lambda} + \frac{1}{\Gamma}\frac{\partial (\Gamma V c)}{\partial \phi} = 0. \tag{3.2}$$

We consider the splitting scheme

$$c_{i,j}^* = c_{i,j}^n + \left( F_{i-\frac{1}{2},j}^n - F_{i+\frac{1}{2},j}^n \right), \tag{3.3}$$

$$c_{i,j}^{n+1} = c_{i,j}^* + \frac{1}{\Gamma_j}\left( \Gamma_{j-\frac{1}{2}} F_{i,j-\frac{1}{2}}^* - \Gamma_{j+\frac{1}{2}} F_{i,j+\frac{1}{2}}^* \right), \tag{3.4}$$

where the 1D fluxes are computed as in Section 2, using Courant numbers

$$\nu_{i\pm\frac{1}{2},j} = \frac{\Delta t}{\Delta \lambda}|U_{i\pm\frac{1}{2},j}| \quad \text{and} \quad \nu_{i,j\pm\frac{1}{2}} = \frac{\Delta t}{\Delta \phi}|V_{i,j\pm\frac{1}{2}}|.$$

(In fact, the limiter in the $\phi$-direction will be slightly modified to incorporate the different factors $\Gamma$ in (3.4), see the appendix.)

The computations are performed on a uniform $2m \times m$ grid with cell centers $(\lambda_i, \phi_j)$ given by $\lambda_i = (i - \frac{1}{2})\Delta\lambda$ and $\phi_j = (j - \frac{1}{2})\Delta\phi - \frac{1}{2}\pi$ for $i = 1, \cdots, 2m$, $j = 1, \cdots, m$ and $\Delta\lambda = \Delta\phi = \pi/m$. The cell boundaries are located at $\lambda_{i+\frac{1}{2}} = \frac{1}{2}(\lambda_i + \lambda_{i+1})$ and $\phi_{j+\frac{1}{2}} = \frac{1}{2}(\phi_j + \phi_{j+1})$. At the poles we have a no-flux condition, that is, $\Gamma_{j\pm\frac{1}{2}} F_{i,j\pm\frac{1}{2}}^* = 0$ for $j \pm \frac{1}{2} = \frac{1}{2}$ or $m + \frac{1}{2}$, reflecting the fact that the physical length of these cell-boundaries is zero. Furthermore, for cells that are

located downstream of the poles the calculation of the fluxes in $\phi$-direction may need values $c^*_{i,j}$ across the poles. These are found by constant extrapolation,

$$c^*_{0,j} = c^*_{1,j}, \quad c^*_{m+1,j} = c^*_{m,j}.$$

(Interpolation, using values across the poles, gave worse results, due to the fact that the $c^*_{i,j}$ are non-physical quantities which are discontinuous across the poles.)

The modified velocities at the cell boundaries will be taken as

$$U_{i\pm\frac{1}{2},j} = \left(U - \frac{1}{2}\Delta t \frac{\partial U}{\partial \lambda} U + \frac{1}{2}\Delta t \frac{\partial U}{\partial \phi} V\right)(\lambda_{i\pm\frac{1}{2}}, \phi_j), \tag{3.5}$$

$$V_{i,j\pm\frac{1}{2}} = \left(V - \frac{1}{2}\Delta t \frac{1}{\Gamma}\frac{\partial(\Gamma V)}{\partial \phi} V - \frac{1}{2}\Delta t\, U \frac{\partial V}{\partial \lambda}\right)(\lambda_i, \phi_{j\pm\frac{1}{2}}). \tag{3.6}$$

These velocities are derived in the same way as for advection on a plane, see formula (2.14), with the aim of achieving second order accuracy in time. However, the derivation is based on Taylor expansions of the error terms. Near the poles these Taylor expansions loose their significance, since the expansions will involve powers of $\Delta t/\Gamma$, instead of genuine powers of $\Delta t$. At the grid points nearest to the pole we have $\Gamma \sim \Delta\phi$, so that the asymptotic considerations are only valid if $\Delta t/\Delta\phi \to 0$.

As we shall see, the scheme is indeed inaccurate near the poles if both $\Delta t$ and $\Delta\phi$ are small. In fact, the local errors near the poles are only slightly smaller than with first-order splitting. Nevertheless, second-order is preferable for accuracy outside the polar regions for deformational flows as in Figure 1. For the errors at the poles some special measures will be considered.

**Remark.** It is clear from the conservation form of (3.3),(3.4) that the scheme will conserve the quantity

$$\Delta\lambda\,\Delta\phi \sum_{i=1}^{2m}\sum_{j=1}^{m} \Gamma_j\, c_{i,j},$$

which approximates the total mass of the concentration field $c$ on the sphere.

*3.2. Solid body rotation test on the sphere*

The reduction of accuracy near the poles is well illustrated with the solid body rotation test of Wiliamson and Rasch [12]. As in [8] we consider a cone shaped initial profile, given by

$$c_0(\lambda, \phi) = \max(0, 1 - r(\lambda, \phi)/R) \tag{3.7}$$

where

$$r(\lambda, \phi) = 2\sqrt{\left(\cos(\phi)\sin(\tfrac{1}{2}(\lambda - \tfrac{3}{2}\pi))\right)^2 + \left(\sin(\tfrac{1}{2}\phi)\right)^2}, \qquad R = 7\pi/m.$$

Here $m$ is the number of grid points in $\phi$-direction, taken as $m = 64$, and $R$ is the base radius of the cone, corresponding to 7 grid points. The center of the cone is $(\frac{3}{2}\pi, 0)$. The velocities in this test are

$$u(\lambda, \phi) = 2\pi\cos(\lambda)\sin(\phi), \quad v(\lambda, \phi) = -2\pi\sin(\lambda). \tag{3.8}$$

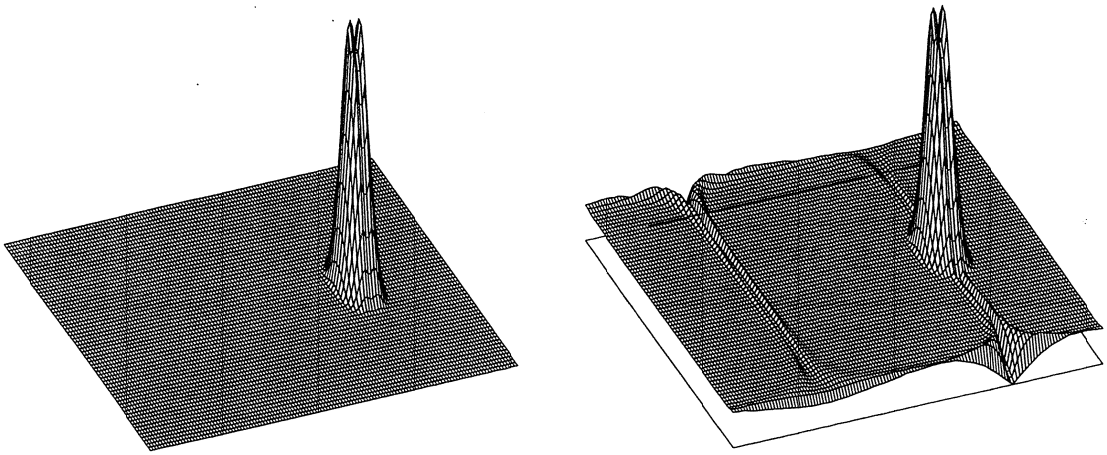

FIGURE 2. Cone tests without background (left) and with background (right).

With this velocity field the cone profile will have completed at time $t = 1$ one full rotation with trajectory over both poles. This will be covered in 256 time steps (maximal Courant numbers $\approx 20$) with the flux-limited splitting scheme.

The left picture of Figure 2 shows a 3D plot of the numerical result on the $\lambda, \phi$-plane after one rotation. We see a strong deformation of the peak, which has crossed both poles.

To gain more insight, it is useful to consider a background concentration. In the right picture of Figure 2 the result is shown for the initial profile

$$\tilde{c}_0(\lambda, \phi) = 0.1 \ + \ 0.9 \ c_0(\lambda, \phi). \tag{3.9}$$

We now see that also the background is strongly deformed as it flows over the poles. In each step an $\mathcal{O}(1)$ error is introduced at the poles, and these errors are advected in the direction of the equator along the streamlines. The errors become less prominent during the advection towards the equator, due to the fact that the area of the cells (on the sphere) become larger.

The errors at the poles are caused by the splitting itself as well as by the approximations for the 1D processes. These errors can be made small by taking a sufficiently small time step, say 1/5120 with maximal Courant number $\approx 1$, but this implies of course a large increase in computational work. In the following sections we will discuss some special measures to suppress the large errors near the poles, while maintaining the computational efficiency.

*3.3. Polar caps and polar mixing*

In [1], Allen et al. considered a splitting scheme where the 1D processes were subject to a CFL restriction. In order to relax this restriction they introduced polar caps, considered as cells with homogeneous distribution. With such polar caps the splitting scheme is applied further away from the poles. This will lead to smaller Courant numbers, and also the splitting errors will become less severe. On the other hand, the polar caps will introduce diffusion for profiles passing the poles, and so these caps should not be taken too large. We note that the 1D scheme used in [1], which was based on [5], is somewhat more diffusive than the present scheme (2.7), (2.8).

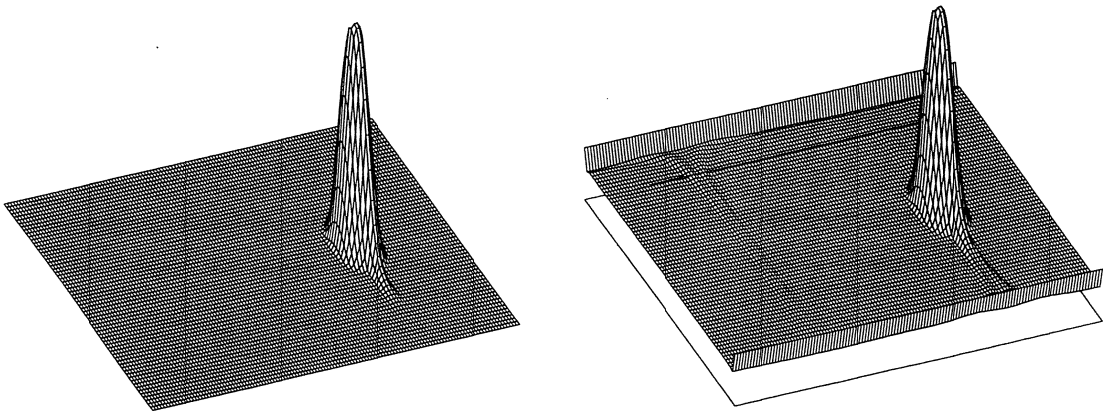

FIGURE 3. Cone tests for polar caps.

In Figure 3 the numerical solutions are shown for polar caps with diameter $2\Delta\phi$ (the first and last row in the plots correspond to values inside the caps). The diffusive effect of the polar caps is clearly seen for the profile without background. The picture with background shows that also the splitting error is still quite large with this time step size. We note that in [1] smaller time steps were taken near the poles.

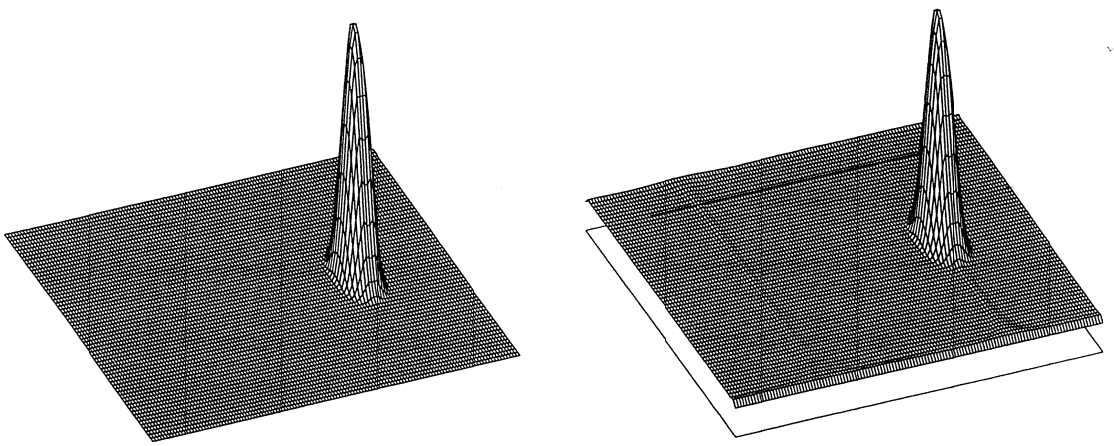

FIGURE 4. Cones test for polar mixing.

By experiments we found that better results are obtained if the scheme is simply applied on the uniform grid, but after each time step the values at the cells adjacent to the poles are mixed, that is, for $j = 1$ and $j = m$ we replace the $c_{i,j}^{n+1}$ by the average value

$$\frac{1}{2m}\sum_{i=1}^{2m} c_{i,j}^{n+1}.$$

We shall refer to this procedure as polar mixing. The difference with the polar caps is that we now have zonal transport inside the caps (that is, transport in the $\lambda$-direction). The results

are shown in Figure 4. Obviously, the splitting error is strongly reduced but also the diffusive effect has nearly disappeared. Although there still is a slight deformation of the background and some inaccuracy at the poles, this seems acceptable for practical purposes.

**Remark.** It is clear from the above figures that the modifications (3.5),(3.6) do not give accurate results at the poles. We note however that without these modifications the results with either polar caps or polar mixing become much worse.

*3.4. Deformation correction*

An other way of reducing the errors near the poles follows from the observation that these errors are already present for the background concentrations. This suggests the following modification: each time the wind field is updated we compute the result of one step of the splitting scheme starting with solution $\equiv 1$. Let us call the result of this one step $\alpha_{i,j}$. Along with this, we also take one step with a non-splitted scheme, again starting with solution $\equiv 1$,

$$\beta_{i,j} = 1 + \frac{\Delta t}{\Delta\lambda}\left(U(\lambda_{i-\frac{1}{2}},\phi_j) - U(\lambda_{i+\frac{1}{2}},\phi_j)\right) + \frac{\Delta t}{\Gamma_j \Delta\phi}\left(\Gamma_{j-\frac{1}{2}} V(\lambda_i,\phi_{j-\frac{1}{2}}) - \Gamma_{j+\frac{1}{2}} V(\lambda_i,\phi_{j+\frac{1}{2}})\right).$$

Next, we store the factors $\delta_{i,j} = \beta_{i,j}/\alpha_{i,j}$, which will be used to correct the splitting scheme. Let the result of the uncorrected splitting step (3.3),(3.4) be denoted by $\bar{c}_{i,j}^{n+1}$. We then correct this value according to

$$c_{i,j}^{n+1} = \delta_{i,j}\, \bar{c}_{i,j}^{n+1} \tag{3.10}$$

and accept this as the new approximation at time level $t_{n+1}$. We note that only near the poles the $\delta_{i,j}$ will differ significantly from 1.

Figure 5 shows the results for the cone tests. The error near the poles now has completely disappeared, and the results are accurate. The scheme appears to be positive but not strictly monotonic (there is a small dip trailing the cone, see also Table 1).

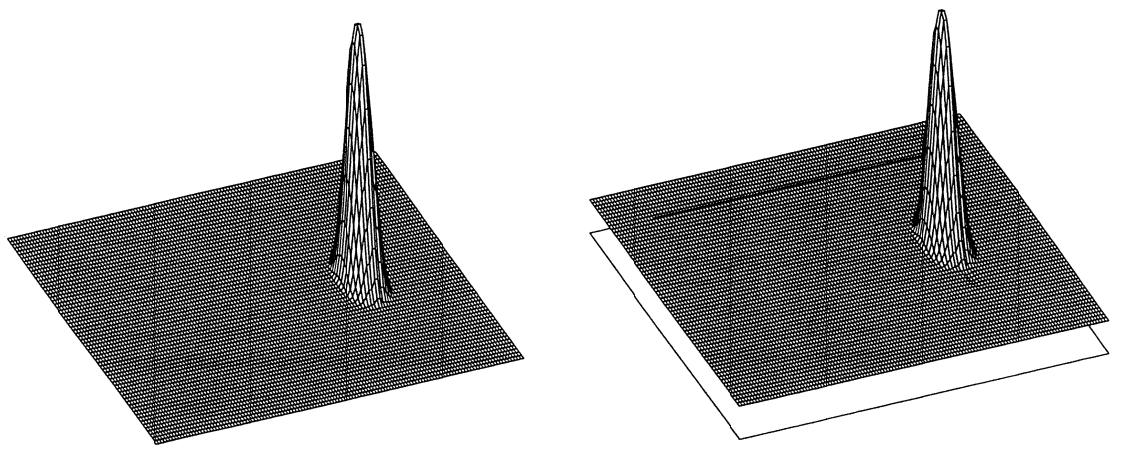

FIGURE 5. Cone tests for deformation correction.

There are two drawbacks with this approach. First, at each update of the wind field the factors $\delta_{i,j}$ have to be computed and stored. Secondly, due to the fact that this is not a

modification on the fluxes, but on the $c_{i,j}$ values, the remaining scheme will no longer be strictly mass-conservative. However, if there are many species to be advected, say 10 or more, or if the wind field is not often updated, then the calculation of the $\delta_{i,j}$ is a relatively small task. Furthermore, in numerical tests we observed that the mass conservation is still almost valid, see for instance the results for ERR1 in Table 1.

*3.5. Accuracy and CPU times*

In Table 1 the errors are listed for two versions of the splitting scheme : Split-PoMx with polar mixing (Figure 4) and Split-DeCo with deformation corrections (Figure 5). Both versions are considered here with and without limiting.

| | EMIN | EMAX | ERR0 | ERR1 | ERR2 | CPU(min) | CPU' |
|---|---|---|---|---|---|---|---|
| *Cone tests* | | | | | | | |
| Donor Cell | 0 | -0.83 | 0.063 | 0 | -0.86 | 6.2 | 1 |
| Split-PoMx (non-lim.) | -0.02 | -0.15 | 0.011 | 0 | -0.09 | 0.63 | 0.10 |
| Split-DeCo (non-lim.) | -0.02 | -0.12 | 0.009 | 0.001 | -0.08 | 0.62 | 0.10 |
| Split-PoMx (limited) | 0 | -0.17 | 0.011 | 0 | -0.12 | 0.83 | 0.13 |
| Split-DeCo (limited) | 0 | -0.15 | 0.009 | 0.001 | -0.11 | 0.80 | 0.13 |
| *Cylinder tests* | | | | | | | |
| Donor Cell | 0 | -0.30 | 0.067 | 0 | -0.023 | 6.2 | 1 |
| Split-PoMx (non-lim.) | -0.05 | 0.06 | 0.029 | 0 | -0.004 | 0.63 | 0.10 |
| Split-DeCo (non-lim.) | -0.03 | 0.07 | 0.028 | $-2 \times 10^{-5}$ | -0.004 | 0.61 | 0.10 |
| Split-PoMx (limited) | -0.06 | 0.02 | 0.028 | 0 | -0.006 | 0.81 | 0.13 |
| Split-DeCo (limited) | -0.02 | 0.02 | 0.028 | $7 \times 10^{-5}$ | -0.006 | 0.80 | 0.13 |

TABLE 1: Results for one revolution around the sphere, 256 time steps for the splitting methods, 5120 time steps for the Donor Cell scheme. The values for the error measures are set 0 if they approach single precision round-off ($< 10^{-6}$).

The results in the table are for the cone shaped profile (3.7) and for a cylinder of height 1, with the same base as the cone, placed on top of a background value 1. The wind field is given by (3.8), and the splitting schemes are again applied with 256 time steps for one full rotation. To enable comparison with the methods used in [8] the same error measures are considered and the standard first-order upwind (donor-cell) scheme has been included with 5120 time steps (maximal Courant number $\approx 1$), which is to be compared with the MPDATA-1,1,0 scheme in [8]. Along with the CPU time in minutes on a SGI workstation, we also have listed the quantity CPU', which is the scaled time with respect to the donor cell scheme.

For completion we give the formulas for the error measures used in Table 1. They represent the errors of the minimum and maximum, the scaled $L_2$-error and the errors in mean value and variance, respectively. The sums and max/min values are taken over $i = 1, \cdots, 2m$, $j =$

$1, \cdots, m$,

$$\text{EMIN} = \frac{\min(c^n_{i,j}) - \min(c^0_{i,j})}{\max(c^0_{i,j})}, \qquad \text{EMAX} = \frac{\max(c^n_{i,j}) - \max(c^0_{i,j})}{\max(c^0_{i,j})},$$

$$\text{ERR0} = \frac{(\sum \gamma_j (c^n_{i,j} - c^0_{i,j})^2)^{1/2}}{\max(c^0_{i,j})}, \qquad \text{ERR1} = \frac{\sum \gamma_j c^n_{i,j}}{\sum \gamma_j c^0_{i,j}} - 1, \qquad \text{ERR2} = \frac{\sum \gamma_j (c^n_{i,j})^2}{\sum \gamma_j (c^0_{i,j})^2} - 1,$$

where $\gamma_j = \Gamma_j / (2m \sum_{k=1}^m \Gamma_k)$. The scaling is chosen such that ERR0 will be equal to 1 if the error is 1 in all grid points and $\max(c^0_{i,j}) = 1$ (we are not completely sure whether this is the same scaling as in [8].)

The results for the cone show that the flux limiter only slightly affects the height of the peak. The limited schemes are positive but approximately 30% more expensive than the non-limited counterparts.

The results for the cylinder with background clearly show that the schemes are not monotone. Even with the limited Split-DeCo scheme there still is a few percent under- and overshoot, see also the contour plots in Figure 7. For the Split-PoMx schemes the largest undershoots occur at the poles, in agreement with Figure 4.

Outside the polar regions the Split-PoMx and Split-DeCo schemes have a comparable accuracy. The Split-DeCo schemes have smaller errors at the poles but they are not strictly mass conserving.

Comparison with the semi-Lagrangian TREMBA schemes used in [8] shows that the splitting schemes are more accurate than the 2-nd order method, but slightly less accurate than the non-limited TREMBA schemes of order 4 and 6. However, with the limited versions of these schemes in [8] the peak height of the cone is strongly reduced and the mass errors become much worse. Also with these schemes limiting is necessary for positivity.

The main advantage of the splitting schemes seems the computational efficiency. The schemes require only a fraction of the CPU time of the donor cell scheme (with 5120 time steps), whereas the limited semi-Lagrangian schemes in [8] appear several times more expensive than the donor cell scheme.

For further comparison we have also included contour plots for the Split-DeCo schemes with the same figure lay-out as in [8]. The isolines are drawn at $0.0 - \epsilon, 0.1 - \epsilon, 0.2 - \epsilon, \cdots$ with $\epsilon = 10^{-4}$ and with solid lines for the numerical solution, dashed lines for the exact solution.

The plots for the cone reveal a small phase error, which is probably introduced at the crossing of the poles. The cylinder test in Figure 7 clearly show that the scheme with limiter is not monotone, but it should be noted that the over- and undershoots are small and the cylinder shape is reasonably well maintained.

In conclusion, both versions of the splitting scheme perform well on this solid body rotation, which was designed specifically to test the suitability of numerical schemes for transport over the poles. Outside the polar regions the transport is similar to planar advection, for which we know that the schemes are efficient and accurate, see [3]. Due to the smaller errors at the poles the Split-DeCo schemes seem to have a slight advantage over the Split-PoMx versions. The flux limiter gives positive solutions without adding much numerical diffusion or clipping

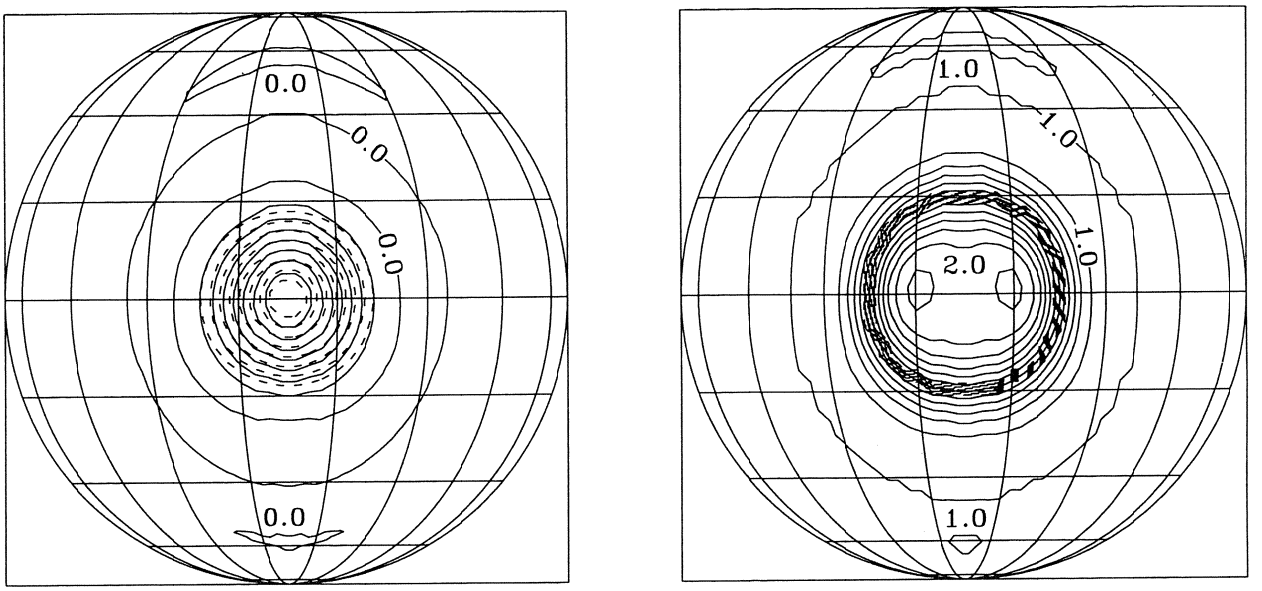


FIGURE 6. Contour plots for Split-DeCo (non-limited) for cone and cylinder.

of peaks. In the near future these schemes will be tested in a more general 3D setting with nonlinear chemistry.

**Remark.** As a further experiment we also considered the wind field

$$u(\lambda,\phi) = \sqrt{2}\,\pi(cos(\phi) + sin(\phi)\cos(\lambda)), \quad v(\lambda,\phi) = -\sqrt{2}\,\pi\sin(\lambda) \tag{3.11}$$

with center of cone and cylinder shifted to $(\pi, 0)$. The profile then travels only over the north-pole but the center does not remain on the same meridian. Again, at $t = 1$ one full rotation has been completed. The numerical results were similar to those in the Figures 4-5 and Table 1, and therefore they are not reproduced here.

APPENDIX : LIMITING FOR MERIDIONAL TRANSPORT

The limiter described in Section 2.1 needs a minor adjustment for the fractional step (3.4), which treats the meridional transport. Without this adjustment small negative values are created (magnitude in the range $10^{-4}$–$10^{-5}$).

In the following we omit the index $i$ and the asterisk in (3.4). Further we assume for the moment that $V > 0$ and that the Courant numbers are at most 1 (the large Courant numbers arise only in the $\lambda$-direction). With limiting we then have, see (2.8),

$$c_j^{n+1} = c_j + \nu_{j-\frac{1}{2}}\frac{\Gamma_{j-\frac{1}{2}}}{\Gamma_j}\left(c_{j-1} + \psi(\nu_{j-\frac{1}{2}},\theta_{j-1})(c_j - c_{j-1})\right)$$

$$-\nu_{j+\frac{1}{2}}\frac{\Gamma_{j+\frac{1}{2}}}{\Gamma_j}\left(c_j + \frac{1}{\theta_j}\psi(\nu_{j+\frac{1}{2}},\theta_j)(c_j - c_{j-1})\right),$$

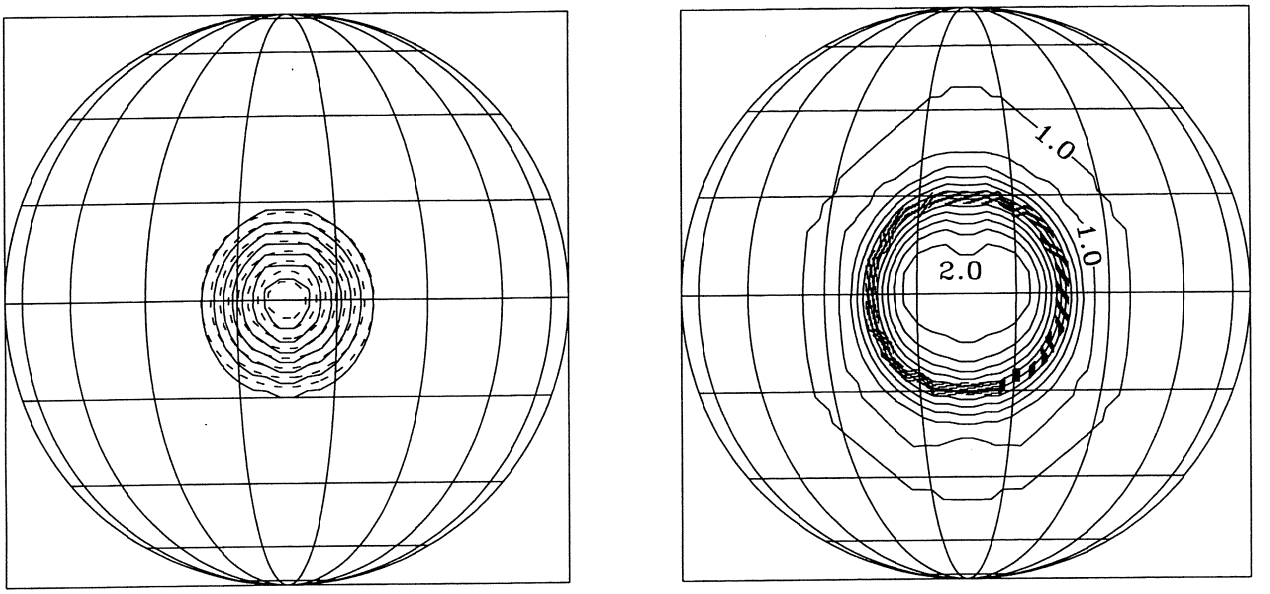


FIGURE 7. Contour plots for Split-DeCo (limited) for cone and cylinder.

which can be written as

$$c_j^{n+1} = Ac_j + Bc_{j-1}$$

with

$$A = 1 + \nu_{j-\frac{1}{2}} \frac{\Gamma_{j-\frac{1}{2}}}{\Gamma_j} \psi(\nu_{j-\frac{1}{2}}, \theta_{j-1}) - \nu_{j+\frac{1}{2}} \frac{\Gamma_{j+\frac{1}{2}}}{\Gamma_j} \left(1 + \frac{1}{\theta_j} \psi(\nu_{j+\frac{1}{2}}, \theta_j)\right),$$

$$B = \nu_{j-\frac{1}{2}} \frac{\Gamma_{j-\frac{1}{2}}}{\Gamma_j} \left(1 - \psi(\nu_{j-\frac{1}{2}}, \theta_{j-1})\right) + \nu_{j+\frac{1}{2}} \frac{\Gamma_{j+\frac{1}{2}}}{\Gamma_j \theta_j} \psi(\nu_{j+\frac{1}{2}}, \theta_j).$$

The requirement for positivity is $A \geq 0, \quad B \geq 0$.

Assume that $\psi(\nu, \theta) = 0$ for $\theta \leq 0$ and $0 \leq \psi(\nu, \theta) \leq 1$. This ensures that $B \geq 0$. The requirement $A \geq 0$ is satisfied if

$$\frac{1}{\theta} \psi(\nu_{j+\frac{1}{2}}, \theta) \leq \frac{1 - \nu'_{j+\frac{1}{2}}}{\nu'_{j+\frac{1}{2}}}, \qquad \nu'_{j+\frac{1}{2}} = \frac{\Gamma_{j+\frac{1}{2}}}{\Gamma_j} \nu_{j+\frac{1}{2}}.$$

This is enforced by replacing in (2.7) the expression $(1 - \nu)\theta/\nu$ by $(1 - \nu')\theta/\nu'$.

Likewise, if $V < 0$ we get the requirement

$$\frac{1}{\theta} \psi(\nu_{j-\frac{1}{2}}, \theta) \leq \frac{1 - \nu''_{j-\frac{1}{2}}}{\nu''_{j-\frac{1}{2}}}, \qquad \nu''_{j-\frac{1}{2}} = \frac{\Gamma_{j-\frac{1}{2}}}{\Gamma_j} \nu_{j-\frac{1}{2}},$$

and so now we replace $(1 - \nu)\theta/\nu$ in (2.7) by $(1 - \nu'')\theta/\nu''$.

By a somewhat tedious calculation, it follows that the limiter will also give positivity in case we have outflow at both cell boundaries, that is, if $V_{j-\frac{1}{2}} < 0$ and $V_{j+\frac{1}{2}} > 0$, provided that both velocities are sufficiently small. This can be considered as a smoothness condition, since $V = 0$ somewhere inside the cell.

REFERENCES


[1] D.J. Allen, A.R. Douglass, R.B. Rood and P.D. Guthrie, *Application of a monotonic upstream-biased transport scheme to three-dimensional constituent transport calculations.* Mon. Wea. Rev. 119 (1991), pp. 2456-2464.

[2] A. Bott, *Monotone flux limitation in the area-preserving flux-form advection algorithm.* Mon. Wea. Rev. 120 (1992), pp. 2595-2602.

[3] W. Hundsdorfer, R.A. Trompert, *Methods of lines and direct discretization: a comparison for linear advection.* Appl. Num. Math. 13 (1993), pp. 469-490.

[4] B. Koren, *A robust upwind discretization for advection, diffusion and source terms.* In : Numerical Methods for Advection-Diffusion Problems, C.B. Vreugdenhil, B. Koren (eds.), Notes on Numerical Fluid Mechanics 45, Vieweg, Braunschweig, 1993.

[5] B. van Leer, *Towards the ultimate conservative difference scheme IV, a new approach to numerical convection.* J. Comput. Phys. 23 (1977), pp. 276-299.

[6] R.J. LeVeque, *Numerical methods for conservation laws, 2-nd edition.* Lectures in Mathematics, ETH Zürich, Birkhäuser Verlag, Basel, 1992.

[7] P.K. Smolarkiewicz, *The multi-dimensional Crowley advection scheme.* Mon. Wea. Rev. 110 (1982), pp. 1968-1983.

[8] P.K. Smolarkiewicz, P.J. Rasch, *Monotone advection on the Sphere: an Eulerian versus semi-Lagrangian approach.* J. Atmos. Sci. 48 (1991), pp. 793-810.

[9] G. Strang, *Trigonometric polynomials and difference methods of maximal accuracy.* J. Math. and Phys. 41 (1962), pp. 147-154.

[10] P.K. Sweby, *High resolution schemes using flux-limiters for hyperbolic conservation laws.* SIAM J. Numer. Anal. 21 (1984), pp. 995-1011.

[11] D.L. Williamson, *Review of numerical approaches for modeling global transport.* In : Air pollution modeling and its applications IX, H. van Dop and G. Kallos (eds.), NATO Challenges of Modern Society 17, Plenum Press, 1992, pp. 377-394.

[12] D.L. Wiliamson, P.J. Rasch, *Two-dimensional semi-Lagrangian transport with shape-preserving interpolation.* Mon. Wea. Rev. 117 (1989), pp. 102-129.

[13] S.T. Zalesak, *A preliminary comparison of modern shock-capturing schemes : linear advection.* In : Advances in Computer Methods for Partial Differential Equations IV, R. Vichnevetsky and R.S. Stapelman (eds.), IMACS, 1987, pp. 15-22.